Hindawi
Advances in Condensed Matter Physics
Volume 2022, Article ID 8961039, 14 pages
https://doi.org/10.1155/2022/8961039

Research Article

Synthesis of $CoFe_2O_4$/Graphene Oxide-Grafted Tetraethylenepentamine for Removal of Cr (VI) from Aqueous Solution

Hui Pan, Donglin Zhao, and Li Wang

Key Laboratory of Functional Molecule Design and Interface Process, Anhui Jianzhu University, Hefei 230601, China

Correspondence should be addressed to Donglin Zhao; zhaodlin@126.com

Received 9 February 2022; Revised 23 April 2022; Accepted 25 April 2022; Published 13 May 2022

Academic Editor: Kiyokazu Yasuda

In this study, amino-functionalized magnetic graphene-based composite TEPA-GO/$CoFe_2O_4$ (TGOM) was prepared by a simple one-step hydrothermal reaction and applied to the removal of Cr (VI) from wastewater. The removal of Cr (VI) by TGOM has the characteristics of high removal efficiency and excellent cycle performance. The maximum adsorption capacity is 114.81 mg/g, and the adsorption efficiency can still reach 62% after four cycles. The mass percentage of amino in TGOM material is about 1.97% according to thermogravimetric analysis. The modification by TEPA increased the adsorption sites and improved the adsorption capacities due to the synergistic effect of chelation with Cr (VI). The effects of pH, contact time, and temperature on the removal of Cr (VI) were studied. The removal process accorded with the pseudo-second-order kinetics and Langmuir isotherm model, and the thermodynamic parameters showed that the adsorption process was exothermic and spontaneous. The characterization analysis before and after adsorption showed that there were complexation reaction, electrostatic adsorption, and reduction mechanism in the removal process. The above results indicate that TGOM is an effective adsorption material for the removal of Cr (VI) in wastewater.

1. Introduction

The rapid development of industry in modern society brings not only economic development but also many pollution problems, one of which is water pollution. In the water pollution system, heavy metal pollution cannot be ignored. It is highly toxic and will pose a major threat to human health and environmental safety even at a very low level [1, 2]. Cr (VI) is a heavy metal ion that exists in many industrial wastewaters and has very high toxicity. It is known that the toxicity of chromium will change with the change of valence [3]. There are mainly two valence states of chromium in nature, namely, Cr (III) and Cr (VI) [4]. As we all know, the toxicity of Cr (VI) is very high, so it is imperative to remove Cr (VI) from wastewater. A variety of methods to remove Cr (VI) in wastewater can be found in previous studies, such as precipitation, adsorption, filtration, and ion exchange. [5–9]. Adsorption is considered as one of the most effective removal methods because of its unique advantages such as low cost, high economic benefit, and safe operation. To this end, scholars have prepared a variety of adsorbents to remove toxic Cr (VI) such as activated carbon [10], related nanomaterials [11], and metal materials [12, 13].

Previous studies have shown that graphene oxide (GO) works well in adsorption material because it is a good two-dimensional structure material with a high surface area and a variety of oxygen-containing functional groups on the surface [14, 15], which can provide a lot of adsorption sites. However, we know that GO is a kind of hydrophilic material, and it may be difficult to separate from water when it is used as an adsorbent [16]. Therefore, the combination of nano-magnetic particles and GO to form a new magnetic adsorption material which can be well separated from water has become a research hotspot in recent years. For example, a magnetic Fe_3O_4/GO nanocomposite was prepared for the adsorption of Cr (VI) in wastewater [17]. It has been

reported that some functional groups (such as amine) can be grafted on the GO surface to improve the adsorption efficiency of GO [18].

According to past experience, $CoFe_2O_4$ magnetic nanoparticles are intended to be loaded on GO to enable rapid separation after adsorption [19]. In order to further increase the adsorption performance of the material, tetraethylenepentamine (TEPA) containing more amino groups can be grafted on the surface of GO to provide more adsorption sites through amino protonation to improve the adsorption of Cr (VI) [18, 20, 21].

In this study, TGOM magnetic nanomaterials were successfully prepared by a simple one-step hydrothermal method, and the morphology, structure, and performance characteristics of the materials were studied through a series of characterizations. The adsorption capacity of Cr (VI) was studied, which is the effect on the adsorption performance under the conditions of different initial pH, adsorption time, and reaction temperature. And on this basis, the recycling ability of the TGOM was further studied.

This study provides a simple preparation method to prepare material (TGOM), and $CoFe_2O_4$ and TEPA are loaded on the GO surface as carrier material, which provides more choices for magnetic and amino group-containing materials that can be loaded. Meanwhile, TGOM also has a good adsorption effect, which can provide a new solution for removing Cr (VI) pollution in water.

2. Experiment Section

2.1. Materials. Graphite powder (30 μm, 99.85%) was produced by the Shanghai Colloid Chemical Plant in China. Concentrated sulfuric acid (H_2SO_4, AR, 98%), phosphoric acid (H_3PO_4, AR, 98%), potassium permanganate ($KMnO_4$, GR, 99.8%), hydrogen peroxide (H_2O_2, AR), ethylene glycol (EG), sodium acetate (NaAc), cobalt chloride hexahydrate ($CoCl_2{\cdot}6H_2O$, AR), iron trichloride hexahydrate ($FeCl_3{\cdot}6H_2O$, AR, 99%), and tetraethylenepentamine (TEPA) were purchased from Shanghai Mike Lin Biochemical Co., Ltd. All the reagents were of analytical grade, and all the water used in the experiment was deionized water.

2.2. Synthesis of TGOM. GO was produced by oxidizing graphite powder. The method of preparing GO in this study is further improved on the basis of the Hummers method [22, 23]. TGOM was prepared by a simple one-step hydrothermal method. Specifically, 0.1 g GO was sonicated for 3 h to make it fully dispersed in 50 mL of EG. Then, 0.54 g of $FeCl_3{\cdot}6H_2O$, 0.24 g of $CoCl_2{\cdot}6H_2O$, 3.69 g NaAc, and 0.42 g TEPA were added to the above solution and stirred continuously for 45 min at room temperature. After that, put the mixed solution into a 100 mL Teflon-lined stainless steel autoclave and keep it at 180°C for 24 hours. Finally, the obtained product was washed, dried, and ground to get the product TGOM. Chen et al. also used the hydrothermal method to synthesize $CoFe_2O_4$-TETA-GO material in previous literature [24], but the process of preparation is divided into two steps. Compared with the preparation route in literature, the synthesis method in this study is more convenient. The composite material MGO ($GO/CoFe_2O_4$) was also prepared by this method for a contrast study.

2.3. Characterization. The morphology of the material was studied by transmission electron microscope (FEI-JSM 6320F, TEM) image (imaging voltage of 200 kV) and scanning electron microscope (JEM-2010, SEM) image (imaging voltage of 10 kV). The functional groups of the material were measured by Fourier transform infrared spectroscopy (FTIR-1500, China; Nicolet 6700, USA) in the range of 400~4000 cm^{-1} by the KBr tablet test. The X-ray diffraction (XRD) was measured on a Bruker D8 X-ray diffraction analyzer, and the diffraction spectrum was recorded in the 2-theta angle range of 10°–80°. The elemental composition and chemical state of the surface changes were analyzed by XPS spectroscopy (PHI-5300, UK) (Mg-Kα X-ray excitation source, corrected binding energy C1 s is 284.8 eV). Raman spectra were recorded by a Raman spectrometer (INVIA, England) with holographic notch filter and CCD detector. Thermogravimetric analysis (Mettler TGA/DSC3+, Switzerland) of the material was carried out in an N_2 atmosphere and at a temperature ranging from room temperature to 600°C (10°C/min).

2.4. Batch Experiments. The prepared TGOM material was used as the adsorbent for the adsorption experiments. The effects of pH, adsorption time, and reaction temperature on the adsorption test were studied. TGOM was dispersed uniformly in deionized water by ultrasonic treatment to make a certain concentration of adsorbent suspension. Then, it was transferred to a PE tube with a known concentration (50 mg/L) of Cr (VI) solution. After adjusting the pH (range 2–10) with 0.1 M HCl and 0.1 M NaOH solution, the temperature was kept at 298 K and oscillated (180 rpm) for 24 h to study the influence of pH on the adsorption experiment. A solution of Cr (VI) to be adsorbed with a certain concentration (20 mg/L, 30 mg/L) was prepared, it was adjusted to the optimal pH value, and then the samples were taken at the same temperature (298 K) and different reaction time (time interval: 0–150 min) for measurement to study the effect of time on adsorption test. The effect of reaction temperature on the experiment is similar to the previous process, only changing the experimental conditions to different temperatures (298 K, 308 K, and 318 K). The adsorbent concentration in all adsorption experiments was 0.1 g/L, and the concentration of Cr (VI) in the adsorbed solution was determined by UV-Vis spectrophotometer (T6 New Century, China). All the experiments in this study are set parallel experiments to ensure the accuracy of experimental data.

Adsorption capacity (q_e) is calculated according to the following formula:

$$q_e = (c_0 - c_e) * \frac{V}{m}, \tag{1}$$

where C_0 (mg/L) is the initial concentration of Cr (VI) in the solution, C_e (mg/L) is the equilibrium concentration, V (L) is

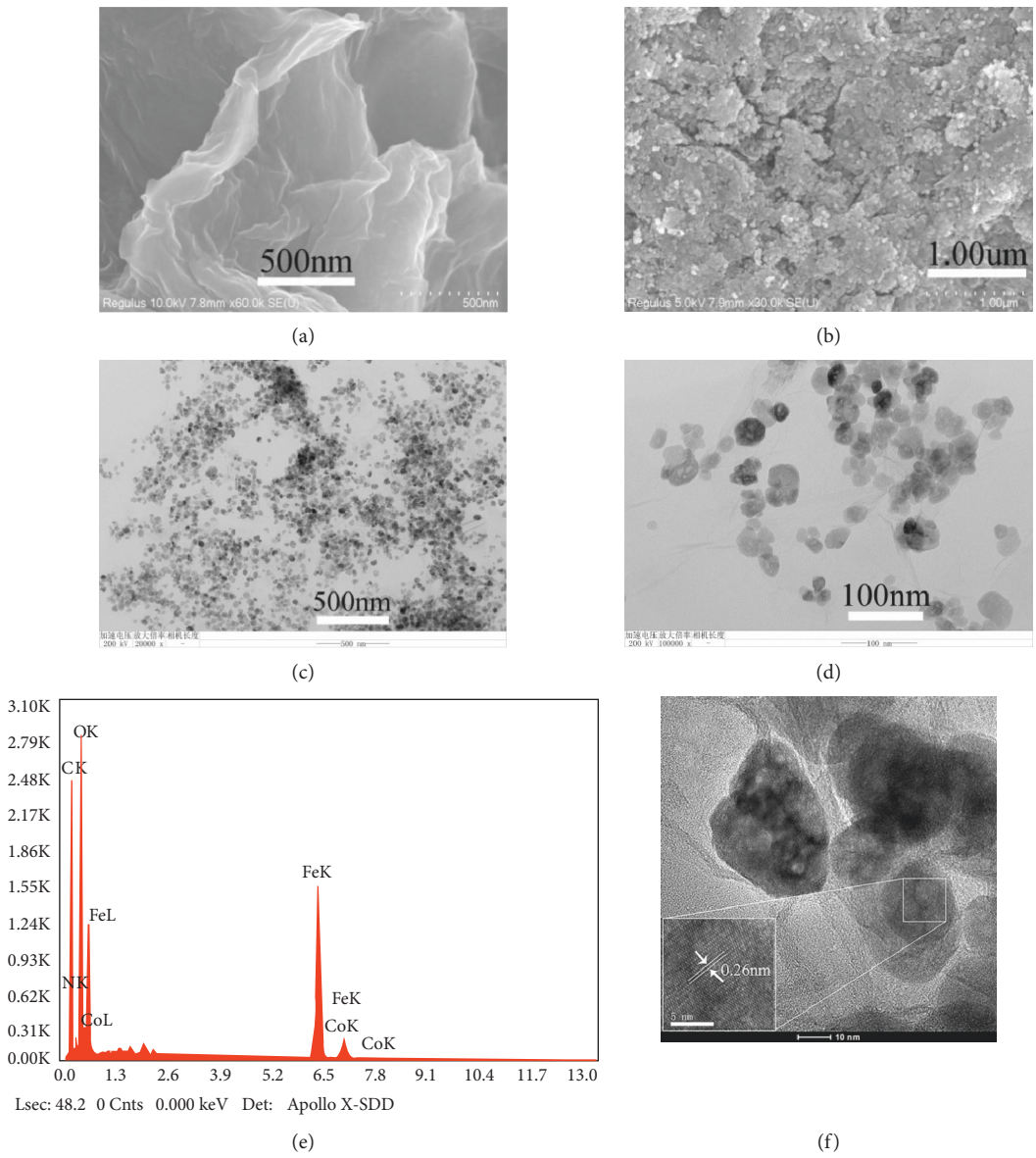

Figure 1: (a, b) SEM images of GO and TGOM; (c, d) TEM images of TGOM; (e) EDS of TGOM; (f) HR-TEM image of TGOM.

the volume of the solution, and m (g) is the mass of the adsorbent TGOM.

3. Results and Discussion

3.1. Characterization. Figure 1 shows the morphology of the sample. It can be observed that GO appears as a sheet with a large number of wrinkles on the surface (Figure 1(a)), which provides a higher surface area and facilitates the loading of nanoparticles on its surface. After loading $CoFe_2O_4$ and TEPA (Figure 1(b)), it can be seen that the granular nanoparticles are uniformly distributed on the GO surface, and the GO surface still maintains a wrinkled morphology, which effectively prevents the aggregation of nanoparticles [25]. Figures 1(c) and 1(d) show the TEM image of the composite TGOM. It can be seen that the metal nanoparticles are effectively distributed on the GO surface, and the particles are uniform. Figure 1(e) shows the EDS energy spectrum analysis diagram of the composite material. It can be seen that there are elements such as Fe, Co, and N on the surface of the material, which further proves that $CoFe_2O_4$ and TEPA are successfully loaded on the surface of GO. The crystal plane spacing measured in the HRTEM diagram (Figure 1(f)) of TGOM is 0.26 nm, which corresponds to the (311) crystal plane of $CoFe_2O_4$ and demonstrates the successful loading of $CoFe_2O_4$.

The XRD pattern of TGOM is shown in Figure 2(a). From Figure 2(a), it can be observed that TGOM has seven distinct characteristic peaks located at $2\theta = 18.33$, 30.17, 35.48, 43.16, 53.54, 57.01, and 62.68°, respectively. Comparing with the standard patterns (JCPDS 22–1086), the seven characteristic peaks correspond to the (111), (220), (311), (400), (422), (511), and (440) planes of $CoFe_2O_4$ [26]. The results indicate that the composite materials TGOM

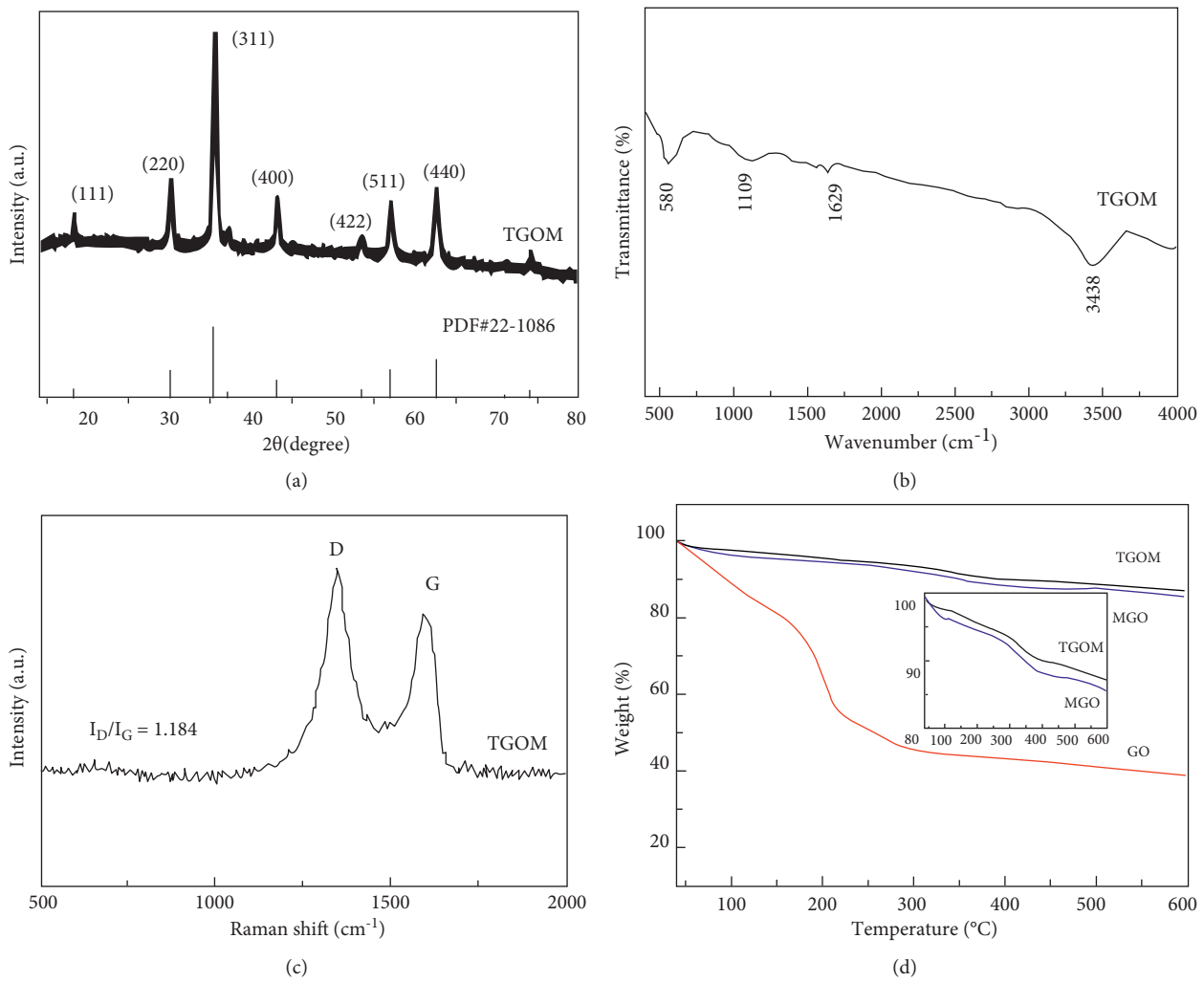

FIGURE 2: (a) XRD pattern of TGOM; (b) FT-IR spectrum of TGOM; (c) Raman spectrum of TGOM; (d) TGA thermogram of GO, MGO, and TGOM.

contain $CoFe_2O_4$ magnetic nanoparticles. According to the Bragg equation ($2d\sin\theta = n\lambda$), the crystal plane spacing of (311) is 0.253 nm, which is similar to the HRTEM result (0.26 nm).

The FT-IR spectrum of the composite TGOM is shown in Figure 2(b), and the functional group changes of TGOM can be seen. In Figure 2(b), the sample has an obvious characteristic peak at about 3438 cm^{-1}, which is the O-H tensile vibration, indicating that the sample contains a small amount of water molecules [27, 28]. In the TGOM spectrum, it can be observed that there is a characteristic peak at 1109 cm^{-1}, corresponding to the tensile vibration of the C-N, and the peak at 1560 cm^{-1} is the bending vibration of N-H [29, 30]. It indicates that the GO surface was successfully loaded with amino groups (TEPA). The characteristic peak at 580 cm^{-1} corresponds to the vibration of the metal-oxygen bond (tetrahedron) [31], which indicates that $CoFe_2O_4$ was also successfully loaded onto the GO surface. The overall FT-IR analysis results show that amino groups were successfully introduced on the surface of GO during the functionalization of GO, and the material is magnetically and easy to separate from the solution. Reading the relevant literature shows that there is no interaction between amino and magnetic particles composited on the surface of GO, such as the amino acid-modified graphene oxide magnetic nanocomposite (AMGO@Fe_3O_4) in the study of Yan et al. [32].

Figure 2(c) shows the Raman spectrum of TGOM, which can be used to further observe the structural changes of the sample. It can be seen from Figure 2(c) that TGOM has two characteristic peaks near 1345 cm^{-1} and 1600 cm^{-1}, which are the D peak (related to disordered vibration of carbon atom sp3) and G peak (related to in-plane vibration of carbon atom sp2), respectively [22, 33]. The intensity ratio of the D peak and the G peak represents the degree of structural defects. The I_D/I_G value of the composite TGOM is 1.184 (Figure 2(c)), and the I_D/I_G value of GO reported in the literature is less than 1 [14, 16], which indicates that GO increases the defect density and disorder degree of the material due to the combination of TEPA and $CoFe_2O_4$.

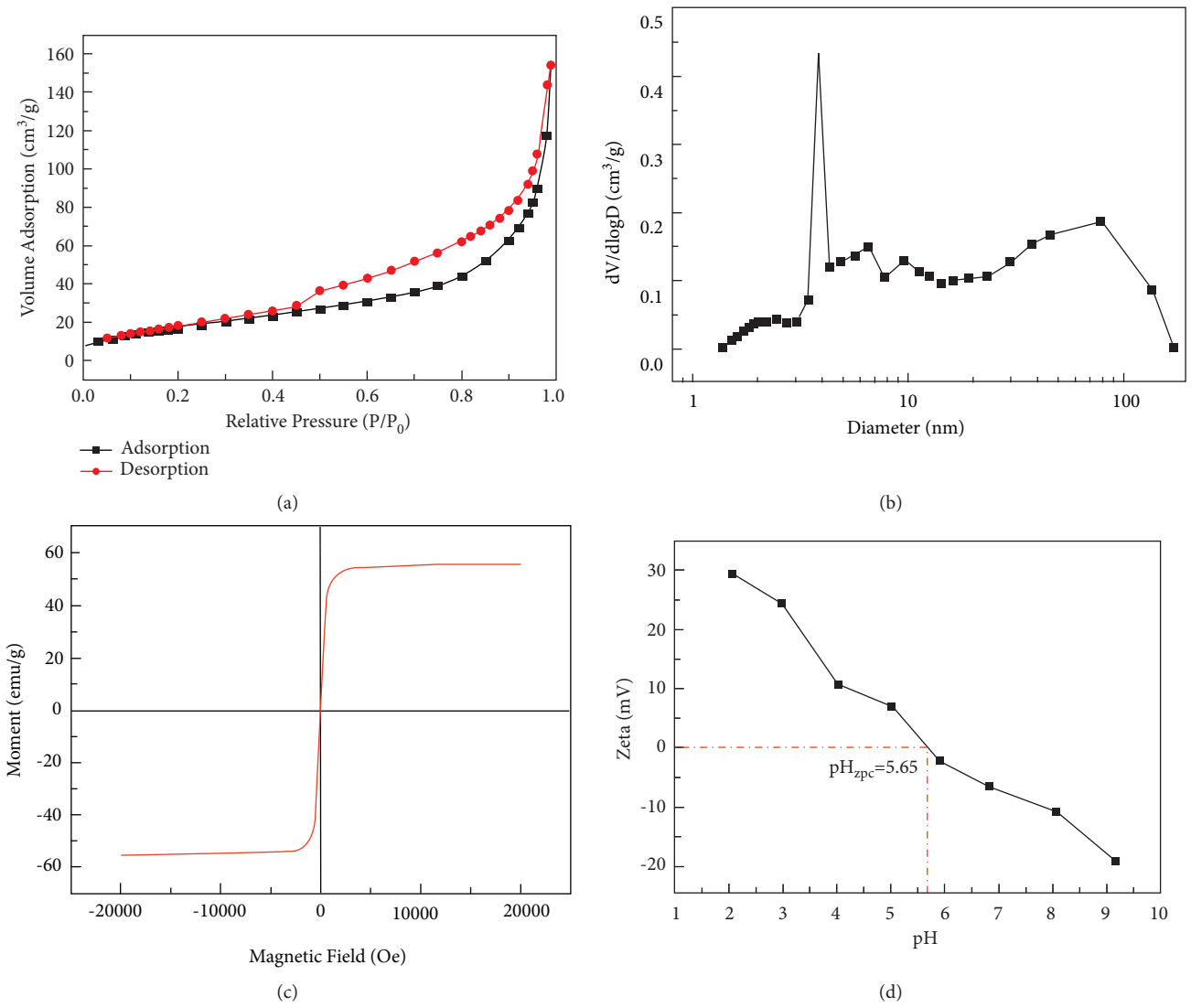

FIGURE 3: (a, b) N_2 adsorption-desorption curves and the pore size distribution curve of TGOM; (c) magnetization curve of TGOM; (d) zeta potential of TGOM.

Figure 2(d) shows the thermal stability study of materials (GO, MGO, and TGOM). In Figure 2(d), the weight of the three samples lost in the first 100°C came from the evaporation of water molecules in the material. For GO, the weight loss at temperatures between 100 and 300°C is due to the decomposition of oxygen-containing functional groups in the sample, while above 300°C is due to the carbon skeleton decomposition [34]. At 600°C, the total weight loss of GO is 61.47 wt%. The weight loss rates of MGO and TGOM were 14.65 wt% and 12.92 wt%, respectively. This proves that both materials have good thermal stability. It can be seen from the illustration that TGOM has higher thermal stability than that of MGO, and its thermal decomposition weight loss is attributed to the evaporation of water in the material and the thermal decomposition of the carbon skeleton [34, 35]. The weight loss process of MGO is similar to that of TGOM. It can be calculated that the mass percentage of $CoFe_2O_4$ in the two materials is about 54.85% and the mass percentage of amino in TGOM material is about 1.97%. It is shown that the thermal stability of the material is improved by the introduction of $CoFe_2O_4$ and TEPA.

Figure 3 shows the BET analysis of the composite material. And the results show that the N_2 adsorption-desorption isotherm of TGOM belongs to a typical IV type curve (Figure 3(a)), indicating that the material has many mesoporous structures [36]. Figure 3(b) shows the pore size distribution diagram, and the average pore size of TGOM is 3.827 nm. According to BET analysis, the specific surface area of TGOM is 64.959 m^2/g and the pore volume is 0.2385 cm^3/g. Figure 3(c) shows the magnetization curve of TGOM. It can be clearly seen that the magnetization value of the material is high (55.5 emu/g), and this indicates that the adsorbent can be recovered using magnetism well after the

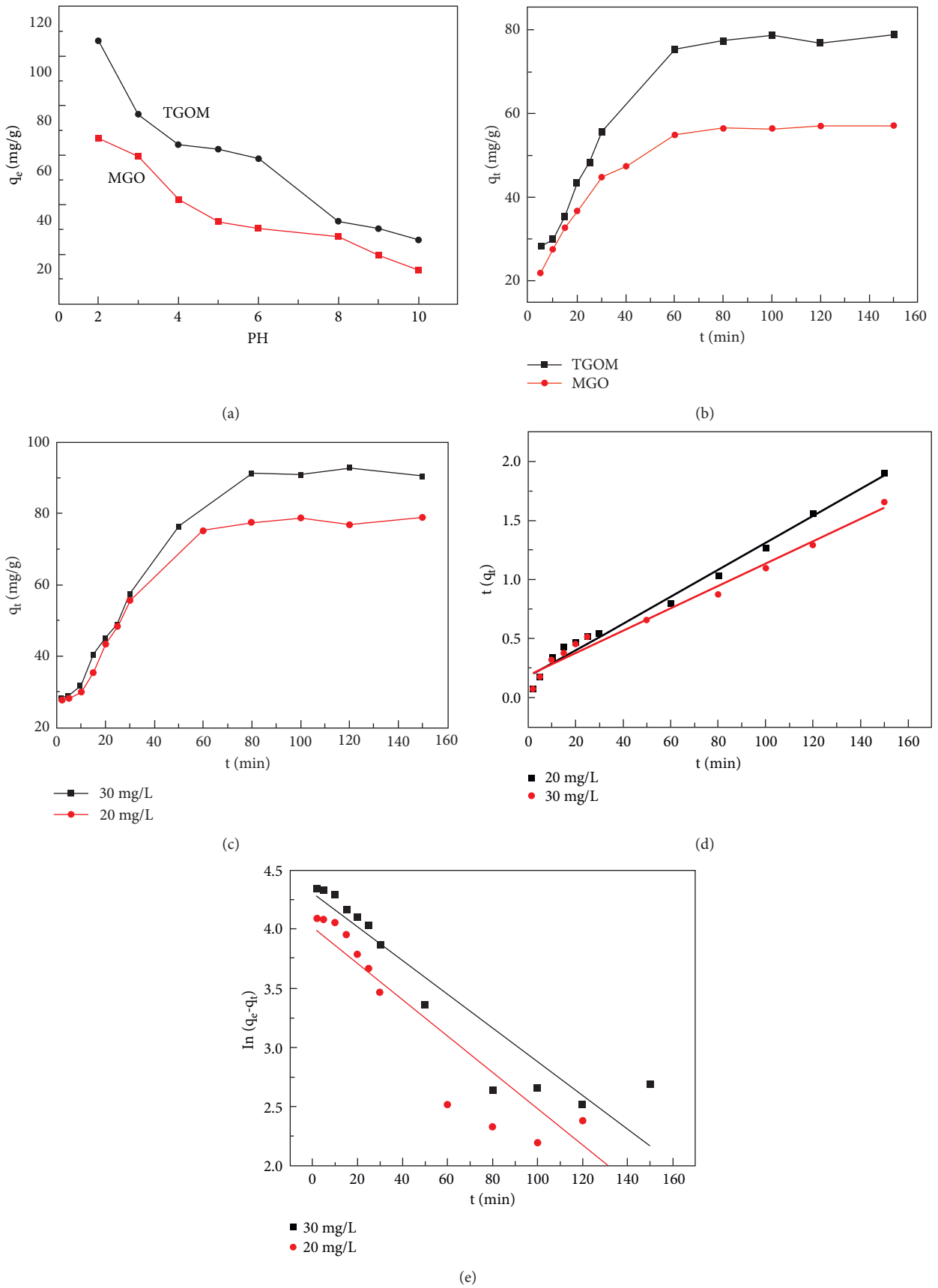

FIGURE 4: (a) Effect of pH on Cr (VI) removal ($T = 298$ K, $C_0 = 50$ mg/L, $m/V = 0.1$ g/L); (b) effect of time on Cr (VI) removal on TGOM and MGO ($T = 298$ K $C_0 = 20$ mg/L, $m/V = 0.1$ g/L, pH = 2); (c) effect of time on Cr (VI) removal at different initial concentration ($T = 298$ K, $m/V = 0.1$ g/L, pH = 2); (d) pseudo-second-order kinetics graph of Cr (VI) removal; (e) pseudo-first-order kinetics graph of Cr (VI) removal.

Table 1: Kinetic parameters for the removal of Cr (VI) on TGOM.

	Pseudo-first-order			Pseudo-second-order		
C_0 (mg/L)	K_1 (min^{-1})	$q_{e,\ mod}$ (mg/g)	R^2	K_2 (g/min/mg)	$q_{e,\ mod}$ (mg/g)	R^2
20	0.1536	55.56	0.8525	0.0007	88.11	0.9867
30	0.1425	74.12	0.8743	0.0005	105.48	0.9782

adsorption reaction is completed [37]. The zeta potential of TGOM under different pH conditions is shown in Figure 3(d). It can be seen that the pH_{zpc} is 5.65. And the zeta potential of TGOM is positive when the pH is before 5.65 and negative after 5.65, which indicates that TGOM can effectively adsorb anions ($HCrO_4^-$, etc.) through electrostatic action under the condition of pH less than 5.65.

3.2. Factors Affecting Removal of Cr (VI)

3.2.1. Effect of Initial pH. The pH value of the solution affects the removal process of Cr (VI). Figure 4(a) shows the adsorption effect of TGOM and MGO on Cr (VI) in an aqueous solution under different pH conditions (within the range of 2–10). The results show that the adsorption capacity of the material changes with the pH of the solution, and the adsorption effect of the material is the best when pH = 2. The amino groups on the surface of the material can be protonated to be positively charged at low pH, which can easily adsorb negatively charged Cr (VI) ($HCrO_4^-$, $Cr_2O_7^{2-}$, and CrO_4^{2-}) through electrostatic attraction [21, 38]. At pH = 2, Cr (VI) in the solution exists mostly as $HCrO_4^-$, so there will be better adsorption. In the range of pH 3–7, although Cr (VI) exists mainly as $HCrO_4^-$ and $Cr_2O_7^{2-}$, the decreased adsorption effect is due to the gradual weakening of amino protonation. Under alkaline conditions, Cr (VI) exists mostly as CrO_4^{2-}, and the deprotonation reaction of the amino group occurs on the material surface, which will produce electrostatic repulsion with CrO_4^{2-}, and thereby, the adsorption effect will gradually decrease [17, 39]. Zhang et al. pointed out that the composite (Fe_3O_4-PEI-SERS) prepared by them has the largest removal of Cr (VI) at pH = 2 [38]. After the optimum pH was determined, the pH conditions of all subsequent experiments were optimal (pH = 2). Figure 4(a) also points out that the removal ability of TGOM is better than that of MGO.

3.2.2. Kinetics Study. Figure 4(b) shows the effect of reaction contact time on Cr (VI) removal. From Figure 4(b), the adsorption of Cr (VI) by TGOM is relatively fast and reaches equilibrium at about 60 min. After that, the adsorption process is not affected by time and tends to be stable. Compared with MGO, the composite material TGOM has a higher adsorption capacity. The influence of different initial concentration on the removal effect in different reaction time (2~160 min) was also studied. As shown in Figure 4(c), when the initial concentration increases, the adsorption capacity also increases. This is because most of the Cr (VI) ions in the solution are more likely to collide with the active sites on the adsorbent surface at a higher initial concentration [40]. On this basis, the pseudo-first-order and pseudo-second-order kinetic models are used to study the kinetics of adsorption reaction. The equations are listed below [41]:

$$\ln\left(q_e - q_t\right) = -K_1 t + \ln\ q_e,$$
$$\frac{t}{q_t} = \frac{t}{q_e} + \frac{1}{K_2 q_e^2}, \tag{2}$$

where K_1 (min^{-1}) and K_2 (g/mg/min) represent the adsorption rate constants of the two models, respectively. t (min) is the contact time of the adsorption reaction, and q_t (mg/g) and q_e (mg/g) represent the t time of the reaction and the amount of Cr (VI) removed by the material when the reaction reaches equilibrium, respectively.

The relevant data obtained by fitting are listed in Table 1. It is pointed out that compared with the pseudo-first-order kinetic model, the rate constants of the pseudo-second-order kinetic model are both more than 0.97 at the two initial concentrations, which proves that the pseudo-second-order model can effectively describe the removal process of Cr (VI) by TGOM. Figure 4(d) shows the fitting curve of the pseudo-second-order kinetic model, and its degree of fit is significantly greater than that of the pseudo-first-order kinetic (Figure 4(e)), which can also prove the above point.

3.2.3. Adsorption Isotherms. The adsorption equilibrium of Cr (VI) on the adsorbent (TGOM) under different initial concentrations and optimal pH was studied. Three different temperatures were investigated in this study. It can be seen from Figure 5(a) that the lower the experimental temperature, the higher the adsorption capacity, which means that there is an exothermic phenomenon in the process of removing Cr (VI) [42]. In order to further study its adsorption behavior, this experiment used Langmuir and Freundlich two typical isotherm models to investigate.

Langmuir model points out that the adsorption process is monolayer adsorption, and its equation is expressed as [42, 43]

$$\frac{C_e}{q_e} = \frac{C_e}{q_{\max}} + \frac{1}{q_{\max} K_L}. \tag{3}$$

Freundlich model points out that the adsorption process is multimolecular layer adsorption, and its equation is expressed as [44, 45]

$$\ln\ q_e = \ln\ K_F + \frac{\ln\ C_e}{n}, \tag{4}$$

where C_e and q_e refer to the concentration (mg/L) and adsorption capacity (mg/g), $q_{\max}$ (mg/g) refers to the maximum adsorption capacity, K_L (L/mg) and K_F

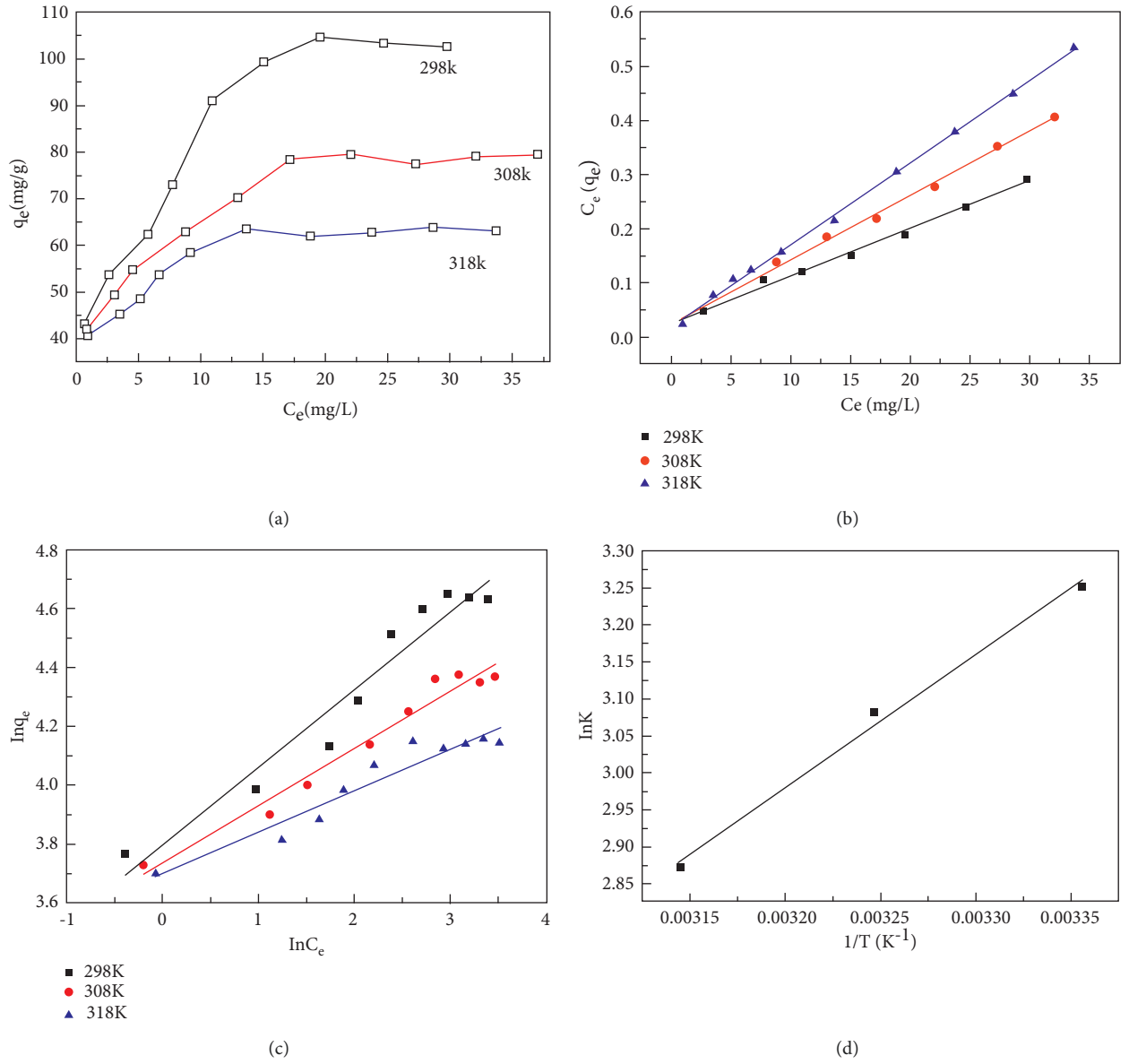

Figure 5: (a) Effect of temperature on Cr (VI) removal (pH = 2, m/V = 0.1 g/L); (b) Langmuir and (c) Freundlich isotherm curves; (d) ln$K$ as a function of 1/T.

Table 2: Parameters of isotherm for Cr (VI) removal by TGOM.

T (k)	Parameter					
	Langmuir			Freundlich		
	q_{max} (mg/g)	K_L·(L/mg)	R^2	n	K_F·(mg^{1-n}·L^n/g)	R^2
298	114.81	0.3366	0.9847	3.79	44.5851	0.9331
308	83.54	0.5135	0.9979	5.14	41.8977	0.9621
318	66.05	0.8175	0.9984	7.12	40.5150	0.9069

(mg^{1-n}·L^n/g) are the adsorption equilibrium constants of the Langmuir model and the Freundlich model, respectively, and n is a constant of the adsorption intensity in the Freundlich model.

Figures 5(b) and 5(c) show the linear fitting plots of the two models, and their parameters are listed in Table 2. It is known from Table 2 that the correlation coefficients (R^2) of the Langmuir model at three temperatures are greater than

Table 3: Comparison of adsorption capacity for removal of Cr (VI) on TGOM with other materials.

Adsorbent materials	pH	Kinetic model	Isotherm model	q_m (mg/g)	Refs.
Amine-functionalized polyacrylonitrile nanofiber (PAN-NH_2)	pH = 2	Pseudo-second-order	Langmuir	156	[39]
Graphene-based adsorbent (ED-DMF-RGO)	pH = 2	—	—	92.15	[46]
Thiol-functional carbon (HT-SCY)	—	Pseudo-second-order	Langmuir	15.41	[47]
Carboxyl-functional carbon (HT-AA)	—	Pseudo-second-order	Langmuir	94.52	[47]
Amino-functional carbon (HT-N)	—	Pseudo-second-order	Langmuir	171.23	[47]
Polyethylenimine-functionalized biosorbent (PEI-ESM)	pH = 3	Pseudo-second-order	Langmuir	160	[48]
Magnetic cyclodextrin-chitosan/graphene oxide (CCGO)	pH = 3	Pseudo-second-order	Langmuir	21.6	[49]
Graphenes magnetic material (Fe_3O_4-GS)	—	Pseudo-second-order	Freundlich	17.29	[50]
Magnetite-polyethylenimine-montmorillonite material (Fe_3O_4-PEIx-MMT)	pH = 3	—	Langmuir	8.8	[51]
TGOM	pH = 2	Pseudo-second-order	Langmuir	114.81	This work

those of the Freundlich model. It can be judged that the removal process of Cr (VI) by TGOM is monolayer adsorption, which is consistent with the Langmuir model [43]. The data in Table 2 also point out that the maximum adsorption capacity of TGOM at 298 K is 114.81 mg/g, which is roughly compared with the adsorption capacity of some other adsorbents in the literature for Cr (VI) in Table 3 [39, 46–51].

Based on the above experiments, the thermodynamic properties of Cr (VI) adsorption by the TGOM was further discussed. And several related thermodynamic parameters were calculated, namely, the change of Gibbs free energy (ΔG), the change of entropy (ΔS), and the change of enthalpy (ΔH). The relevant calculation formula is as follows [52]:

$$\Delta G = -RT \ln K, \tag{5}$$

$$\ln K = -\left(\frac{\Delta H}{R}\right)\frac{1}{T} + \frac{\Delta S}{R}, \tag{6}$$

where T (K) is the temperature, R is the gas constant (8.314 J·mol^{-1}·K^{-1}), and K_d is the thermodynamic equilibrium constant. By finding the linearity between lnK_d ($K_d = q_e/C_e$) and $1/T$, ln$K$ can be obtained when C_e is 0, and then, ΔG can be obtained by Equation (5). Similarly, the values of ΔH and ΔS can be calculated from the slope and intercept of the obtained line by making the linear relation graph of ln$K$ and $1/T$ [53]. Table 4 lists the calculation results. In Table 4, ΔG is negative at the three temperatures and the value of ΔG decreases as the temperature decreases, indicating that the driving force of the adsorption process is greater at low temperatures. So, the TGOM can better remove Cr (VI) at a lower temperature (298 K), which is consistent with the experimental data. The value of ΔH is also negative, which indicates that the process of the adsorption reaction is an exothermic process, and from the result that ΔS is a negative value, the adsorption process is a process of reduced chaos (decrease in entropy) [54].

3.3. Removal Mechanism of Cr (VI) by TGOM. Figure 6 shows the change in Cr concentration in the solution after the reaction. It shows that the change in Cr (VI) and total Cr is similar, and the solution after the reaction contains Cr (III), which indicates that a small amount of Cr (VI) is reduced to Cr (III) during the removal process.

Table 4: Thermodynamic parameters for Cr (VI) removal by TGOM.

T (K)	Parameter		
	ΔG (KJ/mol)	ΔH (KJ/mol)	ΔS (J/mol/K)
298	−8.0565		
308	−7.8921	−14.92	−22.96
318	−7.5944		

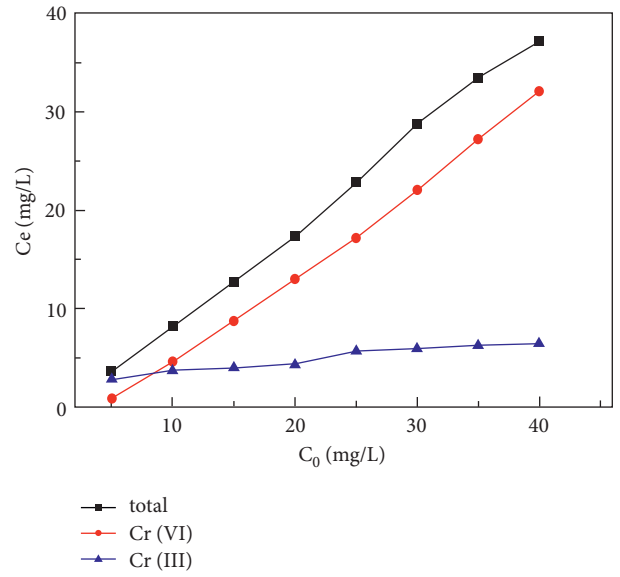

Figure 6: Residual concentration of Cr (total, VI, and III) after reaction in solution.

The XPS spectra of the TGOM before and after the reaction are shown in Figure 7. Figure 7(a) is the overall XPS spectra of TGOM before and after the reaction. Compared with the spectrum before the reaction, the spectrum after the reaction shows the peak of the Cr element, which indicates that TGOM successfully adsorbed chromium on its surface. The O1 s peaks before and after

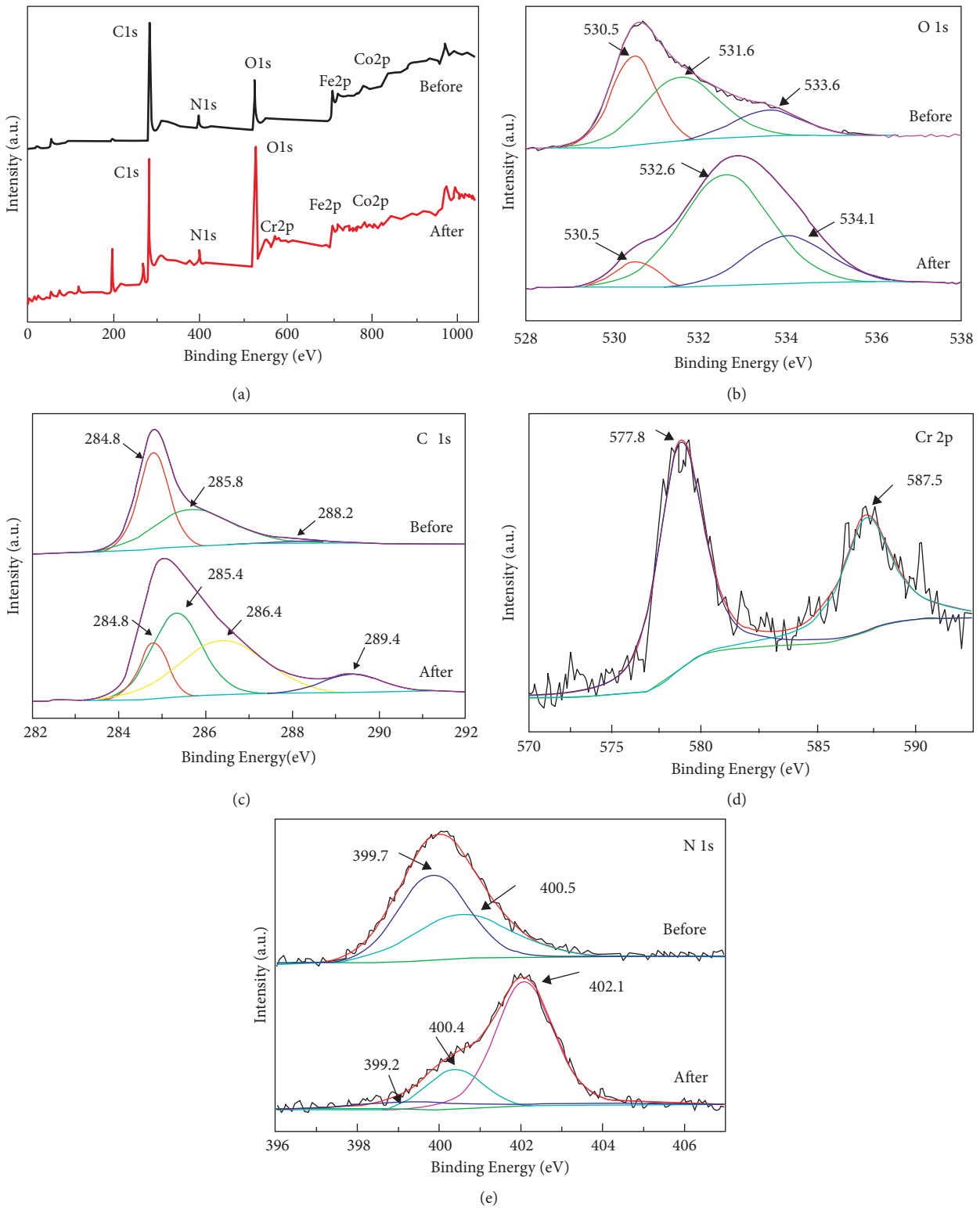

Figure 7: (a) XPS spectra of TGOM before and after adsorption of Cr (VI) and high-resolution XPS survey of (b) O 1 s, (c) C 1 s, (d) Cr 2p, and (e) N 1 s.

the reaction were changed (Figure 7(b)). The characteristic peaks of O1 s appeared at about 530.5, 531.6, and 536.6 eV in the spectrum before the reaction, corresponding to divalent anion oxygen (O^{2-}), hydroxyl (OH^{-}), and oxygen in the water molecule (H_2O) adsorbed by the material [55], respectively. However, it can be seen that after the reaction, the O^{2-} had a significantly lower peak strength and OH^{-} and H_2O peaks improved remarkably, which indicates that

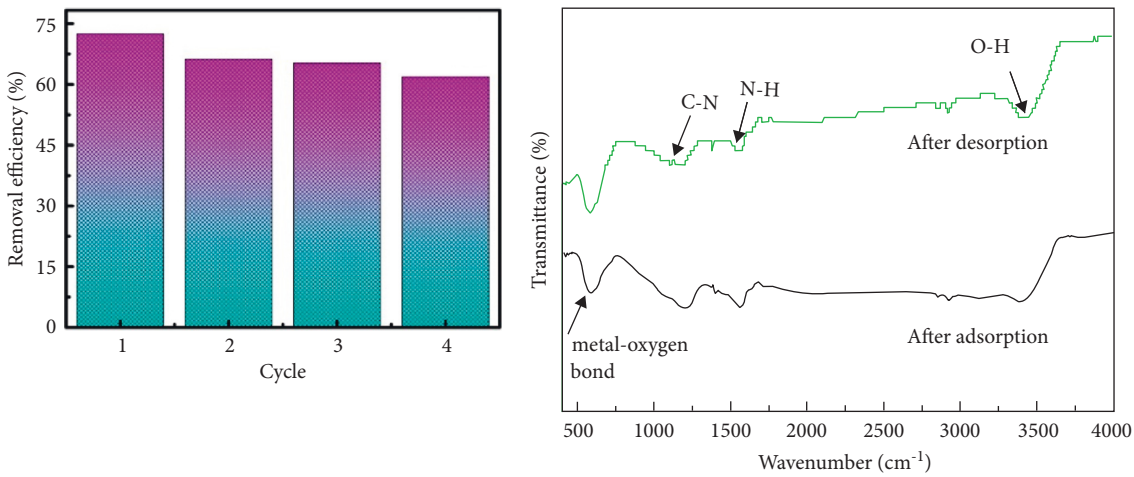

FIGURE 8: (a) Cyclic adsorption of Cr (VI) on TGOM ($T = 298$ K pH = 2, $m/V = 0.1$ g/L, $C_0 = 10$ mg/L); (b) FT-IR of TGOM after adsorption and desorption.

the oxidation degree of the material is relatively low and the stability is good after reaction [56].

There are three peaks of 284.8, 285.8, and 288.2 eV in the spectrum of C1 s before reaction (Figure 7(c)), which correspond to the characteristic peaks of C-C/C=C, C-N, and C-O [57], respectively. It can be seen from the spectrum after the reaction that the peak of C-C/C=C is strongly weakened, while the other peaks are enhanced. Moreover, a characteristic peak corresponding to C-O (286.4 eV) is generated, indicating that a small amount of carbon rings in GO participated in the reaction during the adsorption process [58, 59]. Two peaks corresponding to $Cr2p_{3/2}$ and $Cr2p_{1/2}$ can be observed at approximately 577.8 and 587.5 eV (Figure 7(d)), which correspond to the characteristic peaks related to Cr (III) and Cr (VI), respectively [47, 60, 61]. This indicates that TGOM can reduce part of the toxic Cr (VI) to Cr (III) in the removal of Cr (VI). It can be clear that π electrons on the six-membered ring of carbon in GO participate in the reduction reaction on the basis of the above analysis [46].

Figure 7(e) shows the XPS spectra before and after the reaction of N1 s. From Figure 7(e), it can be seen that there are two peaks at 399.8 and 400.7 eV on the spectrum without reaction, corresponding to the N element in -N=(imine) and -NH- respectively, which proves that this study successfully introduced N onto the GO surface [62]. In the spectrum after the reaction, the peak intensities of the two peaks are observed to be weakened, which indicates that complexation occurred during the adsorption process [63]. In addition, a new characteristic peak appeared at 402.1 eV, which corresponds to the protonated amino group (–N = $^+$) [21], and the protonated amino group (–N = $^+$) can absorb negatively charged Cr (VI) ions through electrostatic reaction [38].

3.4. Regeneration of TGOM. The regenerative cycle performance of the adsorbent determines whether the adsorbent can be practically applied in the real environment. And whether the adsorbent (TGOM) can be regenerated is discussed by studying the adsorption and desorption process. The recovered adsorbent was soaked in 0.1 MNaOH solution for 2-3 h to desorb Cr (VI) adsorbed on the material after the experiment, and then, repeated washing with deionized water was used to wash away the alkali attached on the surface of the material. The regeneration experiment was repeated in this way. The adsorption efficiency of TGOM decreased slightly from 72.5% to 62% after four regeneration experiments (Figure 8(a)). This indicates that TGOM has good reproducible cycle performance.

In order to explore the changes of TGOM during the cycle experiment, FT-IR characterization of TGOM was performed (after adsorption and desorption) as shown in Figure 8(b). Firstly, it can be observed that compared with the FT-IR spectrum before adsorption (Figure 2(b)), the absorption peaks of O-H and metal-oxygen bonds on the surface of TGOM after adsorption and desorption do not change much, which indicates that the material has a better stability. Secondly, compared with before adsorption (Figure 2(b)), the peaks of C-N and N-H in the spectrum after adsorption have slight changes, which indicates that the amino group on the surface of TGOM participates in the adsorption reaction (complexation reaction) during the adsorption process. However, in the spectrum after desorption, it can be seen that the peaks of C-N and N-H do not change much compared with the Figure 2(b), and this indicates that the desorption of the material is successful, that is, the material after desorption can continue to carry out adsorption reaction.

4. Conclusion

In this study, TGOM was successfully prepared by a simple method (one-step hydrothermal method). Material characterization analysis (SEM, XRD, FT-IR, TGA, etc.) proved that TGOM is an adsorbent material with many functional groups on the surface, good thermal stability, and strong

magnetism. The adsorption experiments showed that the optimum pH value for Cr (VI) removal by TGOM was 2, and the adsorption process conformed to the pseudo-second-order kinetic model and the Langmuir isotherm model. The adsorption process of Cr (VI) by TGOM was an exothermic and spontaneous process. The XPS characterization analysis of TGOM indicated that the removal of Cr (VI) was achieved through electrostatic action, complexation reaction, and reduction during adsorption. Cycling experiments demonstrate that TGOM had high removal efficiency and good cycle performance for Cr (VI). In summary, TGOM has the advantages of a simple preparation method, environmental friendliness, high removal efficiency, and good cycle performance. Therefore, it is feasible to use TGOM to remove Cr (VI) in wastewater.

Data Availability

The raw data required to reproduce these findings cannot be shared at this time as the data also form part of an ongoing study.

Conflicts of Interest

The authors declare that they have no conflicts of interest.

Acknowledgments

The financial supports from the National Natural Science Foundation of China (21876001) and Special Support Plan of Anhui Province and Collaborative Innovation Project of Universities in Anhui Province (GXXT-2021-012) are acknowledged.

References

[1] S. Y. Yang, X. Y. Xiao, and E. Tao, "Removing low concentration of Cr (III) from wastewater: using titanium dioxide surface modified montmorillonite as a selective adsorbent," *Inorganic Chemistry Communications*, vol. 125, Article ID 108464, 2021.

[2] Y. L. F. Musico, C. M. Santos, M. L. P. Dalida, and D. F. Rodrigues, "Improved removal of lead (II) from water using a polymer-based graphene oxide nanocomposite," *Journal of Materials Chemistry*, vol. 1, no. 11, pp. 3789–3796, 2013.

[3] L. Y. Hu, L. X. Chen, M. T. Liu, A. J. Wang, L. J. Wu, and J. J. Feng, "Theophylline-assisted, eco-friendly synthesis of PtAu nanospheres at reduced graphene oxide with enhanced catalytic activity towards Cr (VI) reduction," *Journal of Colloid and Interface Science*, vol. 493, pp. 94–102, 2017.

[4] S. Rapti, D. Sarma, S. A. Diamantis et al., "All in one porous material: exceptional sorption and selective sensing of hexavalent chromium by using a Zr^{4+} MOF," *Journal of Materials Chemistry*, vol. 5, no. 28, pp. 14707–14719, 2017.

[5] J. O. Kim and J. Chung, "Implementing chemical precipitation as a pretreatment for phosphorus removal in membrane bioreactor-based municipal wastewater treatment plants," *KSCE Journal of Civil Engineering*, vol. 18, no. 4, pp. 956–963, 2014.

[6] S. Chung, S. Kim, J. O. Kim, and J. Chung, "Feasibility of combining reverse osmosis-ferrite process for reclamation of metal plating wastewater and recovery of heavy metals," *Industrial & Engineering Chemistry Research*, vol. 53, no. 39, pp. 15192–15199, 2014.

[7] B. W. Sung, K. H. Chu, S. L. Yun et al., "Removal of iron and manganese ions from abandoned neutral or alkaline mine drainage via ozone oxidation and micro-sand filtration: a pilot-scale operation," *Desalination and Water Treatment*, vol. 53, no. 9, pp. 2354–2362, 2015.

[8] H. A. Maturana, I. M. Peric, B. L. Rivas, and S. Amalia Pooley, "Interaction of heavy metal ions with an ion exchange resin obtained from a natural polyelectrolyte," *Polymer Bulletin*, vol. 67, no. 4, pp. 669–676, 2011.

[9] Y. Zhao, J. R. Peralta-Videa, M. L. Lopez-Moreno, M. Ren, G. Saupe, and J. L. Gardea-Torresdey, "Kinetin increases chromium absorption, modulates its distribution, and changes the activity of catalase and ascorbate peroxidase in mexican palo verde," *Environmental Science and Technology*, vol. 45, no. 3, pp. 1082–1087, 2011.

[10] R. M. Schneider, C. F. Cavalin, M. A. S. D. Barros, and C. R. G. Tavares, "Adsorption of chromium ions in activated carbon," *Chemical Engineering Journal*, vol. 132, pp. 355–362, 2007.

[11] S. M. Ponder, J. G. Darab, and T. E. Mallouk, "Remediation of Cr (VI) and Pb (II) aqueous solutions using supported, nanoscale zero-valent iron," *Environmental Science and Technology*, vol. 34, no. 12, pp. 2564–2569, 2000.

[12] E. Alvarez-Ayuso, A. Garcia-Sanchez, and X. Querol, "Adsorption of Cr (VI) from synthetic solutions and electroplating wastewaters on amorphous aluminium oxide," *Journal of Hazardous Materials*, vol. 142, pp. 191–198, 2007.

[13] L. Z. Liu, J. J. Xue, X. Y. Shan, G. He, X. Wang, and H. Chen, "In-situ preparation of three-dimensional Ni@graphene-Cu composites for ultrafast reduction of Cr (VI) at room temperature," *Catalysis Communications*, vol. 75, pp. 13–17, 2016.

[14] J. Wang, Z. M. Chen, and B. L. Chen, "Adsorption of polycyclic aromatic hydrocarbons by graphene and graphene oxide nanosheets," *Environmental Science and Technology*, vol. 48, no. 9, pp. 4817–4825, 2014.

[15] Z. H. Cheng, J. Liao, B. Z. He et al., "One-step fabrication of graphene oxide enhanced magnetic composite gel for highly efficient dye adsorption and catalysis," *ACS Sustainable Chemistry & Engineering*, vol. 3, no. 7, pp. 1677–1685, 2015.

[16] S. Bai, X. P. Shen, X. Zhong et al., "One-pot solvothermal preparation of magnetic reduced graphene oxide-ferrite hybrids for organic dye removal," *Carbon*, vol. 50, no. 6, pp. 2337–2346, 2012.

[17] Y. L. Lei, F. Chen, Y. J. Luo, and L. Zhang, "Three-dimensional magnetic graphene oxide foam/Fe_3O_4 nanocomposite as an efficient absorbent for Cr (VI) removal," *Journal of Materials Science*, vol. 49, no. 12, pp. 4236–4245, 2014.

[18] T. S. Anirudhan, S. Jalajamony, and S. S. Sreekumari, "Adsorption of heavy metal ions from aqueous solutions by amine and carboxylate functionalised bentonites," *Applied Clay Science*, vol. 65-66, pp. 67–71, 2012.

[19] M. A. Gabal, K. M. Abou Zeid, A. A. El-Gendy, and M. S. El-Shall, "One-step novel synthesis of $CoFe_2O_4$/graphene composites for organic dye removal," *Journal of Sol-Gel Science and Technology*, vol. 89, no. 3, pp. 743–753, 2019.

[20] S. P. Kuang, Z. Z. Wang, J. Liu, and Z. C. Wu, "Preparation of triethylene-tetramine grafted magnetic chitosan for adsorption of Pb (II) ion from aqueous solutions," *Journal of Hazardous Materials*, vol. 260, pp. 210–219, 2013.

[21] Z. H. Chang, X. G. Sang, Y. Song, X. Q. Sun, and X. X. Liu, "Immobilization of phosphotungstate through doping in

polypyrrole for supercapacitors," *Dalton Transactions*, vol. 48, no. 20, pp. 6812–6816, 2019.

[22] W. Shen, B. Y. Ren, K. Cai, Y. F. Song, and W. Wang, "Synthesis of nonstoichiometric $Co_{0.8}Fe_{2.2}O_4$/reduced graphene oxide (rGO) nanocomposites and their excellent electromagnetic wave absorption property," *Journal of Alloys and Compounds*, vol. 774, pp. 997–1008, 2019.

[23] Y. J. Yao, S. D. Miao, S. Z. Liu, L. P. Ma, H. Sun, and S. Wang, "Synthesis, characterization, and adsorption properties of magnetic Fe_3O_4@graphene nanocomposite," *Chemical Engineering Journal*, vol. 184, pp. 326–332, 2012.

[24] X. J. Sun, F. N. Chen, J. Z. Wei, F. M. Zhang, and S. Y. Pang, "Preparation of magnetic triethylene tetramine-graphene oxide ternary nanocomposite and application for Cr (VI) removal," *Journal of the Taiwan Institute of Chemical Engineers*, vol. 66, pp. 328–335, 2016.

[25] Y. X. Ma, Y. F. Li, G. H. Zhao et al., "Preparation and characterization of graphite nanosheets decorated with Fe_3O_4 nanoparticles used in the immobilization of glucoamylase," *Carbon*, vol. 50, no. 8, pp. 2976–2986, 2012.

[26] M. A. Gabal, A. A. Al-Juaid, S. El-Rashed, and M. A. Hussein, "Synthesis and characterization of nano-sized $CoFe_2O_4$ via facile methods: a comparative study," *Materials Research Bulletin*, vol. 89, pp. 68–78, 2017.

[27] X. Y. Ge, J. J. Li, H. D. Wang, C. Zhang, Y. Liu, and J. Luo, "Macroscale superlubricity under extreme pressure enabled by the combination of graphene-oxide nanosheets with ionic liquid," *Carbon*, vol. 151, pp. 76–83, 2019.

[28] P. T. L. Huong, L. T. Huy, V. N. Phan, M. H. Nam, and V. D. Lam, "Application of graphene oxide-$MnFe_2O_4$ magnetic nanohybrids as magnetically separable adsorbent for highly efficient removal of arsenic from water," *Journal of Electronic Materials*, vol. 45, no. 5, pp. 2372–2380, 2016.

[29] S. Yang, W. B. Yue, D. Z. Huang, C. Chen, H. Lin, and X. Yang, "A facile green strategy for rapid reduction of graphene oxide by metallic zinc," *RSC Advances*, vol. 2, no. 23, pp. 8827–8832, 2012.

[30] N. A. Travlou, G. Z. Kyzas, N. K. Lazaridis, and E. A. Deliyanni, "Functionalization of graphite oxide with magnetic chitosan for the preparation of a nanocomposite dye adsorbent," *Langmuir*, vol. 29, no. 5, pp. 1657–1668, 2013.

[31] V. Mahdikhah, S. Saadatkia, S. Sheibani, and A. Ataie, "Outstanding photocatalytic activity of $CoFe_2O_4$/rGO nanocomposite in degradation of organic dyes," *Optical Materials*, vol. 108, Article ID 110193, 2020.

[32] M. Yan, Q. L. Liang, W. Wan, Q. Han, S. Y. Tan, and M. Ding, "Amino acid-modified graphene oxide magnetic nanocomposite for the magnetic separation of proteins," *RSC Advances*, vol. 7, no. 48, pp. 30109–30117, 2017.

[33] K. N. Kudin, B. Ozbas, H. C. Schniepp, R. K. Prud'homme, I. A. Aksay, and R. Car, "Raman spectra of graphite oxide and functionalized graphene sheets," *Nano Letters*, vol. 8, no. 1, pp. 36–41, 2008.

[34] T. Ahmed, S. N. Xiu, L. J. Wang, and A. Shahbazi, "Investigation of Ni/Fe/Mg zeolite-supported catalysts in steam reforming of tar using simulated-toluene as model compound," *Fuel*, vol. 211, pp. 566–571, 2018.

[35] G. B. Huang, S. Q. Wang, P. A. Song, C. Wu, S. Chen, and X. Wang, "Combination effect of carbon nanotubes with graphene on intumescent flame-retardant polypropylene nanocomposites," *Composites Part A: Applied Science and Manufacturing*, vol. 59, pp. 18–25, 2014.

[36] X. P. Wang, J. Lu, B. Y. Cao et al., "Facile synthesis of recycling Fe_3O_4/graphene adsorbents with potassium humate for Cr (VI) removal," *Colloids and Surfaces A: Physicochemical and Engineering Aspects*, vol. 560, pp. 384–392, 2019.

[37] P. B. Liu, Y. Huang, and X. Zhang, "Superparamagnetic Fe_3O_4 nanoparticles on graphene-polyaniline: synthesis, characterization and their excellent electromagnetic absorption properties," *Journal of Alloys and Compounds*, vol. 596, pp. 25–31, 2014.

[38] S. L. Zhang, Z. K. Wang, H. Y. Chen et al., "Polyethylenimine functionalized Fe_3O_4/steam-exploded rice straw composite as an efficient adsorbent for Cr (VI) removal," *Applied Surface Science*, vol. 440, pp. 1277–1285, 2018.

[39] M. Avila, T. Burks, F. Akhtar et al., "Surface functionalized nanofibers for the removal of chromium (VI) from aqueous solutions," *Chemical Engineering Journal*, vol. 245, pp. 201–209, 2014.

[40] A. B. Albadarin, C. Mangwandi, A. H. Al-Muhtaseb, G. M. Walker, S. J. Allen, and M. N. Ahmad, "Kinetic and thermodynamics of chromium ions adsorption onto low-cost dolomite adsorbent," *Chemical Engineering Journal*, vol. 179, pp. 193–202, 2012.

[41] C. H. Wu, "Adsorption of reactive dye onto carbon nanotubes: equilibrium, kinetics and thermodynamics," *Journal of Hazardous Materials*, vol. 144, pp. 93–100, 2007.

[42] Q. Zhang, D. L. Zhao, S. J. Feng et al., "Synthesis of nanoscale zero-valent iron loaded chitosan for synergistically enhanced removal of U (VI) based on adsorption and reduction," *Journal of Colloid and Interface Science*, vol. 552, pp. 735–743, 2019.

[43] C. T. Hsu, C. H. Chang, and S. Y. Lin, "Comments on the adsorption isotherm and determination of adsorption kinetics," *Langmuir*, vol. 13, no. 23, pp. 6204–6210, 1997.

[44] W. Rogers and M. Sclar, "A modification of the freundlich adsorption isotherm," *Journal of Physical Chemistry*, vol. 36, no. 8, pp. 2284–2291, 2002.

[45] C. D. Hatch, J. S. Wiese, C. C. Crane, K. J. Harris, H. G. Kloss, and J. Baltrusaitis, "Water adsorption on clay minerals as a function of relative humidity: application of BET and freundlich adsorption models," *Langmuir*, vol. 28, no. 3, pp. 1790–1803, 2012.

[46] Y. W. Zhang, H. L. Ma, J. Peng, M. L. Zhai, and Z. Z. Yu, "Cr (VI) removal from aqueous solution using chemically reduced and functionalized graphene oxide," *Journal of Materials Science*, vol. 48, no. 5, pp. 1883–1889, 2013.

[47] L. Q. Liu, W. Q. Cai, C. X. Dang et al., "One-step vapor-phase assisted hydrothermal synthesis of functionalized carbons: effects of surface groups on their physicochemical properties and adsorption performance for Cr (VI)," *Applied Surface Science*, vol. 528, Article ID 146984, 2020.

[48] B. Liu and Y. M. Huang, "Polyethyleneimine modified eggshell membrane as a novel biosorbent for adsorption and detoxification of Cr (VI) from water," *Journal of Materials Chemistry*, vol. 21, no. 43, pp. 17413–17418, 2011.

[49] L. L. Li, L. L. Fan, M. Sun et al., "Adsorbent for chromium removal based on graphene oxide functionalized with magnetic cyclodextrin-chitosan," *Colloids and Surfaces B: Biointerfaces*, vol. 107, pp. 76–83, 2013.

[50] X. Y. Guo, B. Du, Q. Wei et al., "Synthesis of amino functionalized magnetic graphenes composite material and its application to remove Cr (VI), Pb (II) Hg (II), Cd (II) and Ni (II) from contaminated water," *Journal of Hazardous Materials*, vol. 278, pp. 211–220, 2014.

[51] I. Larraza, M. López-Gónzalez, T. Corrales, and G. Marcelo, "Hybrid materials: magnetite–polyethylenimine–montmorillonite, as magnetic

adsorbents for Cr (VI) water treatment," *Journal of Colloid and Interface Science*, vol. 385, no. 1, pp. 24–33, 2012.

[52] Y. Liu, "Is the free energy change of adsorption correctly calculated?" *Journal of Chemical & Engineering Data*, vol. 54, no. 7, pp. 1981–1985, 2009.

[53] S. Kumar, R. R. Nair, P. B. Pillai, S. N. Gupta, M. A. R. Iyengar, and A. K. Sood, "Graphene oxide-$MnFe_2O_4$ magnetic nanohybrids for efficient removal of lead and arsenic from water," *ACS Applied Materials & Interfaces*, vol. 6, no. 20, pp. 17426–17436, 2014.

[54] M. S. Gasser, G. H. A. Morad, and H. F. Aly, "Batch kinetics and thermodynamics of chromium ions removal from waste solutions using synthetic adsorbents," *Journal of Hazardous Materials*, vol. 142, pp. 118–129, 2007.

[55] Y. Zhang, M. Yang, X. M. Dou, H. He, and D. S. Wang, "Arsenate adsorption on an Fe-Ce bimetal oxide adsorbent: role of surface properties," *Environmental Science and Technology*, vol. 39, no. 18, pp. 7246–7253, 2005.

[56] Y. Y. Wang, D. L. Zhao, S. J. Feng, Y. Chen, and R. Xie, "Ammonium thiocyanate functionalized graphene oxide-supported nanoscale zero-valent iron for adsorption and reduction of Cr (VI)," *Journal of Colloid and Interface Science*, vol. 580, pp. 345–353, 2020.

[57] M. R. Islam, D. Joung, and S. I. Khondaker, "Schottky diode via dielectrophoretic assembly of reduced graphene oxide sheets between dissimilar metal contacts," *New Journal of Physics*, vol. 13, no. 3, Article ID 035021, 2011.

[58] Y. X. Ma, P. Q. La, W. J. Lei, C. P. Lu, and X. Y. Du, "Adsorption of Hg (II) from aqueous solution using amino-functionalized graphite nanosheets decorated with Fe_3O_4 nanoparticles," *Desalination and Water Treatment*, vol. 57, no. 11, pp. 5004–5012, 2016.

[59] Y. Wang, X. Liu, H. F. Wang, G. Xia, W. Huang, and R. Song, "Microporous spongy chitosan monoliths doped with graphene oxide as highly effective adsorbent for methyl orange and copper nitrate ($Cu(NO_3)_2$) ions," *Journal of Colloid and Interface Science*, vol. 416, pp. 243–251, 2014.

[60] X. Q. Li, J. S. Cao, and W. X. Zhang, "Stoichiometry of Cr (VI) immobilization using nanoscale zerovalent iron (nZVI): a study with high-resolution X-ray photoelectron spectroscopy (HR-XPS)," *Industrial & Engineering Chemistry Research*, vol. 47, no. 7, pp. 2131–2139, 2008.

[61] L. Xiang, C. G. Niu, N. Tang et al., "Polypyrrole coated molybdenum disulfide composites as adsorbent for enhanced removal of Cr (VI) in aqueous solutions by adsorption combined with reduction," *Chemical Engineering Journal*, vol. 408, Article ID 127281, 2021.

[62] J. Ding, L. T. Pu, Y. F. Wang et al., "Adsorption and reduction of Cr (VI) together with Cr (III) sequestration by poly-aniline confined in pores of polystyrene beads," *Environmental Science and Technology*, vol. 52, no. 21, pp. 12602–12611, 2018.

[63] Q. R. Zhang, Y. X. Li, Q. G. Yang et al., "Distinguished Cr (VI) capture with rapid and superior capability using polydopamine microsphere: behavior and mechanism," *Journal of Hazardous Materials*, vol. 342, pp. 732–740, 2018.